

NEUTRINO ASTRONOMY: Physics Goals, Detector Parameters*

T.K. Gaisser

Bartol Research Institute, University of Delaware
Newark, DE 19716 USA

September 2, 2018

1 Introduction

Observing astrophysical neutrinos opens a new window on the Universe. The claim is already justified by measurement of solar neutrinos and by Supernova 1987A. Several new detectors are in operation or under construction to study in detail the energy range from a few MeV to tens of GeV. The primary focus of a kilometer-scale detector will be to observe neutrinos at higher energy.

After reviewing the energetics of extragalactic cosmic rays, which are closely related to energetic neutrinos in most scenarios, I list some possible sources that have been suggested and describe their neutrino signatures. Next I discuss the nature of the neutrino signals and how they can be detected. The summary section includes some remarks on the prospects for actually finding signals of high energy astrophysical neutrinos. I also comment on the backgrounds of atmospheric neutrinos, which may also serve as a calibration source.

Apart from a brief mention of diffuse galactic neutrinos, I focus in this talk on neutrinos associated with the highest energy cosmic rays, which are assumed to be of extragalactic origin. I also do not address here the important subject of neutrinos from decay of neutralinos, which was covered in David Schramm's talk. (See also Ref. [1] for a recent treatment of the subject.)

2 Extragalactic cosmic radiation

High energy neutrinos require the presence of energetic hadrons. It is therefore of interest to use the observed energy density in cosmic rays to estimate the level of neutrinos that might be

*Talk given at the OECD Megascience Forum Workshop, Taormina, Italy, 22/23 May 1997. Work supported in part by the U.S. Department of Energy.

expected. I discuss the extragalactic component of the cosmic radiation and corresponding extragalactic sources of neutrinos. An analogous argument can be made for sources inside the galaxy [2].

Fig. 1¹ shows the cosmic-ray spectrum with an assumed extragalactic component fitted above the “ankle” and a GZK cutoff around 5×10^{19} eV. The energy content of this component is $\sim 3 \times 10^{-19}$ erg cm^{-3} , assuming an extrapolation to low energy with an E^{-2} differential spectrum. (The total energy content would be higher if the spectrum of the extragalactic component below the ankle is steeper.) The power required to generate this energy density in 10^{10} yrs is $\sim 3 \times 10^{37}$ erg/s per (Mpc)³. This works out to

- $\sim 3 \times 10^{39}$ erg/s per galaxy,
- $\sim 3 \times 10^{42}$ erg/s per cluster of galaxies,
- $\sim 2 \times 10^{44}$ erg/s per active galaxy, or
- $\sim 2 \times 10^{52}$ erg per cosmological Gamma Ray Burst (GRB).

The coincidence between these numbers and the observed energy output of these objects in other wavelengths, especially in the last two cases, is the basis for their use as models of origin of the highest energy cosmic rays.

Suppose now that there is the same energy density in neutrinos, $\rho_E \sim 3 \times 10^{-19}$ erg/ cm^3 with a spectrum

$$E_\nu \frac{dN}{dE_\nu} = A E^{-\gamma} \text{ cm}^{-2} \text{ s}^{-1} \text{ sr}^{-1} \quad (1)$$

that continues to a maximum neutrino energy, E_{max} . Then

$$\int A E_\nu^{-\gamma} dE_\nu = \frac{c}{4\pi} \rho_E \quad (2)$$

normalizes the (diffuse) neutrino flux. The resulting signal depends on the neutrino spectrum. For $\gamma = 1$ and $E_{max} \sim 10^8$ GeV the rate of neutrino-induced muons is about 50 per km^2 per year and depends only weakly on E_{max} . For $\gamma = 0$ up to the same E_{max} the corresponding number is 20 events per year, with the rate nearly inversely proportional to E_{max} .

3 Possible sources and their neutrino signatures

Is there a physical realization of a source that would produce approximately equal energy densities in cosmic-rays and neutrinos? Consider a generic source in which protons and electrons are accelerated to high energy at shocks. The acceleration process is fast but the charged particles remain trapped in the diffuse, turbulent magnetized plasma until they radiate photons, the electrons by bremsstrahlung and the protons by photoproduction. Neutrons from $p + \gamma \rightarrow n + \pi^0$ escape to become cosmic-rays. Neutrinos from charged pions will

¹From Ref. [3] with the addition of data from Tibet [4].

Table 1: Diffuse neutrino rates

| Source | $\nu \rightarrow \mu$ per km ² yr. | E_μ (TeV) (median) | $\nu_e + \bar{\nu}_e$ (total rate per km ³) | $\bar{\nu}_e e^-$ only |
|-----------------|--|---------------------------|--|------------------------|
| Atmospheric | 5×10^5 | 0.1 | | |
| Neutralinos | $< 10^4$ | < 0.1 | | |
| Prompt μ | 400– $\sim 10^4$ | 0.4 | | |
| Galactic center | 300–1000 | 0.4 | | |
| Galaxy clusters | < 5000 | 1.8 | < 3000 | < 50 |
| GRB sources | 200 | 7 | 40 | 10 |
| AGN jets | 500 | 15 | 70 | 200 |
| AGN cores | $< 3 \times 10^4$ | 2 | < 5000 | < 25 |
| GZK | < 1 | 500 | | |
| Top. Defects | < 1 | 5000 | | |

have an energy comparable to the energy in escaping cosmic-rays. The neutrino/ γ -ray ratio, among other things, reflects the ratio of accelerated electrons to protons in the source. This is a crude generic description of some models of AGN jets [5, 6].

Many of the suggested sources of extragalactic cosmic rays including AGN [7], clusters of galaxies [8, 9, 10, 11], cosmological gamma-ray bursts [12] and radiation from topological defects [13] also imply a correlated flux of high energy neutrinos. In addition, there will be neutrinos at some level from cosmic-ray interactions on the 2.7 °K background radiation [14].

In Fig. 2 and Table 1 I summarize the event rates in a kilometer-cubed detector from various sources of high-energy neutrinos. The figure displays the rates for neutrino-induced muons and the table includes events generated by electron-neutrinos as well, including separately the rate of events at the Glashow resonance. The diffuse fluxes referred to here are obtained by integrating over all sources in the Universe for each model (e.g. all blazars or all GRB, etc.). A discussion of the relation between signals from individual point sources and the corresponding diffuse fluxes will be made elsewhere [15]. Generally, the signal rate from a nearby point source will be significantly lower than the corresponding diffuse signal, as illustrated by the example of 3C273 in Ref. [2].

4 Neutrino signals

It is clear from Table 1 and Fig. 2 that some discrimination on neutrino energy will be needed to see the signals of high-energy neutrino sources above the local atmospheric backgrounds. The rate of neutrino-induced muons is given by

$$\frac{d \text{Rate}}{d \ln E_\nu} = \text{Area}(\theta) \times \frac{dN_\nu}{d \ln E_\nu} \times P_{\nu \rightarrow \mu}(E_\nu, E_{\mu, \min}), \quad (3)$$

where

$$P_\nu = \int_{E[\mu, min]}^{E[\nu]} N_A \frac{d\sigma_\nu(E_\nu)}{dE_\mu} dE_\mu \quad (4)$$

$$\sim N_A \sigma_\nu(E_\nu) Range[(1 - \langle y \rangle)E_\nu], \quad (5)$$

where N_A is Avogadro's number and y is the fraction of energy to hadrons in a charged current interaction of a ν_μ (or $\bar{\nu}_\mu$). The last line of this equation allows one to make reasonably accurate estimates easily which display the dependence of the signal on neutrino energy, as in Fig. 2. To display the dependence on muon energy it is straightforward to include the convolution of the differential cross section with the neutrino range as obtained, for example, from Ref. [16].

For results here I have used the cross sections tabulated by Gandhi et al. [17]. The corresponding interaction length of neutrinos is shown in Fig. 3. Note that the Earth, which is 1.1×10^5 km.w.e. along a diameter, partially obscures upward neutrinos with $E_\nu > 100$ TeV. Fig. 4 is an example of the convolution of a predicted diffuse neutrino flux [12] with the projected area (assumed to be 1 km^2) times P_ν . The bottom panel shows the differential rate integrated over the entire upward hemisphere with the effect of absorption by the Earth represented by the shading. Note that this effect leads to an angular dependence for neutrinos with $E > 100$ TeV because the vertically upward neutrinos are absorbed.

For illustrative purposes, I use a simplified treatment of the range that displays the essential physical effects of muon propagation. The energy-loss rate is

$$\frac{dE_\mu}{dX} = -\alpha - E/\xi, \quad (6)$$

with $\epsilon_{critical} = \alpha\xi \sim 500$ GeV. The first term in Eq. 6, which varies slowly with energy, represents ionization loss, while the last term represents radiative losses due to pair production, bremsstrahlung and hadronic interactions. At the critical energy ϵ the two energy loss terms are equal. The solution for the average energy is

$$E(X) \sim (E_0 + \epsilon) \exp[-X/\xi] - \epsilon, \quad (7)$$

and the range R (neglecting fluctuations) is obtained by setting $E(R) = 0$:

$$R \approx \xi \ln(1 + E_0/\epsilon), \quad (8)$$

with $\xi \approx 2$ km water equivalent. (See Ref. [16] for a nice discussion of the effect of fluctuations, the effect of which depends on the neutrino spectrum. Formulas and tables for muon energy loss in various media are given in Ref. [18].)

The muon range is shown in Fig. 5 as a function of its initial energy. It is interesting that for $E_{\mu,0} > 0.5$ TeV $R > 1$ km. Thus for TeV (and higher energy) neutrinos the effective volume for neutrino-induced muons is larger than the physical volume of the detector even for a kilometer-cubed detector. This is the reason that this mode of detection is of such great interest.

A charged-current interaction of a ν_μ (or $\bar{\nu}_\mu$) can occur anywhere between the full range away from the detector to just outside (or perhaps inside) the detector volume. Thus the distance a detected muon has traveled before reaching the detector has a median

$$R_{\frac{1}{2}} \approx \frac{1}{2} \xi \ln(1 + E_0/\epsilon), \quad (9)$$

with a flat distribution. The corresponding distribution of energies at the detector is therefore very broad with a median

$$E_\mu(\text{median}) \approx \epsilon \sqrt{(1 + E_0/\epsilon)} - \epsilon. \quad (10)$$

The right-hand curve in Fig. 5 represents this relation. For example, the median energy at the detector of a muon that starts with 4 TeV is 1 TeV, while for 200 TeV it is 10 TeV. For $E_\mu \gg \epsilon$ $E_\mu(\text{median}) \approx \sqrt{\epsilon E_0}$.

As a specific example, I consider the blazar model of diffuse fluxes of Protheroe [6]. Fig. 6 shows the differential rate on linear (upper panel) and logarithmic (lower panel) scales. Absorption in the Earth has been included. The thin solid line is the background of atmospheric neutrinos exclusive of prompt neutrinos. The dashed lines give minimal and maximal estimates of the prompt neutrino background, which I will discuss further below. A similar model by Mannheim [5] produces a similar, but somewhat lower, signal.

A typical neutrino-induced muon from this spectrum will have initial energy of ~ 1000 TeV, for which the median energy at the detector is ~ 20 TeV. What will such a muon look like as it propagates through the detector? The answer is shown in Figs. 7 and 8, made from calculations by Todor Stanev. They show the propagation history of two individual muons through 1 km of water. In each case the upper panel is on a linear scale and the lower is the same event on a logarithmic scale. What is plotted is the total number of electrons and positrons along the track. Each burst generates an air shower with typical length in water of 5 m. Since for each subshower

$$E_{\text{shower}} \approx 1 \text{ GeV} \times \text{Size at maximum} \quad (11)$$

for showers in this energy range, the vertical axis can also be read as number of GeV deposited per burst.

The examples shown are for $E_\mu = 10$ TeV and $E_\mu = 100$ TeV at the detector. The radiative processes approximately scale with energy in this region, so we can summarize the situation by noting that a muon with $E_\mu \gg \text{TeV}$ will typically generate a couple of bursts per kilometer in which it radiates about 10 per cent of its energy. This is the characteristic signature that a km^3 detector should be sensitive to.

5 Discussion

5.1 Some other sources

The original estimate of diffuse neutrinos from cores of radio quiet AGN [19, 20, 21] is still of interest. Though the highest predictions of Szabo and Protheroe [21] are above the Frejus

limit [22] and the possibility of neutrinos from radio quiet AGN has been overshadowed by the spectacular results from Whipple, HEGRA etc. [23, 24] on high energy gamma-rays from blazars, the model itself could still be valid. The upper limit allowed by Frejus is indicated by the upper dotted line in Fig. 2.

At a lower level, in addition to the diffuse fluxes from AGN jets, there could be production of neutrinos by cosmic rays interacting with gas in clusters of galaxies [10]. The upper dashed curve in Fig. 2 is the signal from maximum allowed flux of Ref. [11] if the same source accounts for the diffuse extragalactic γ -ray fluxes above 100 MeV. Estimates based on cosmic-ray power of current normal galaxies and AGN are considerably lower than this maximum. Achieving this upper limit would require a significant “bright phase” of cosmic-ray production at early epochs.

GRB sources could also produce an interesting flux of diffuse neutrinos if they are the sources of extragalactic cosmic rays [12], as shown by the lowest dotted curve in Fig. 2 and also in Fig. 4.

Another possibility is our own galactic center. This is of special interest because of the recent Egret observation [25] that the spectrum from the central region of the galaxy is harder than would be expected if the γ -rays were produced from cosmic-rays with the differential spectrum of -2.7 observed locally. The lowest dashed curve in Fig. 2 is normalized to the Egret data at ≈ 2 GeV extrapolated to higher energy with a differential index of 2.5 and assuming a similar spectrum of neutrinos (from decay of charged pions). A more quantitative fit [26] to the whole spectrum, including bremsstrahlung photons as well as photons from decay of π^0 s, gives an even harder spectrum at high energy and a correspondingly higher neutrino signal.

5.2 Atmospheric neutrinos: a calibration source

The idea here is to use the atmospheric neutrinos and their known angular dependence [27, 28] to calibrate the neutrino detector. See Fig. 9 for examples of the angular dependence. Since high energy diffuse sources may also have a similar angular dependence (depending on their energy spectra) due to absorption in the earth, some selection on energy will be important. There is a useful discussion of the interplay between energy threshold and angular dependence of high energy signals and lower energy background in Ref. [29], which also discusses the contribution of neutrinos from decay of charmed particles to the atmospheric background.

5.3 Charm

The limiting factor, both for using the atmospheric neutrinos for calibration and in the search for diffuse sources is the uncertainty in the component of prompt neutrinos. The paper of Thunman et al. [30] gives a thorough review of prompt neutrinos, which come primarily from decay of charmed hadrons.² The work of Volkova et al. [31] gives another view (larger

²Because of the steep rise of the structure functions at small x , heavy flavors are always produced predominantly at threshold in hadronic collisions, so production of beauty will always be suppressed relative to

cross section) of prompt neutrinos. The lower dashed line in Fig. 6 gives the contribution of prompt neutrinos from charm as calculated in Ref. [30] assuming only gluon-gluon fusion to be effective in producing charm. The upper dashed curve indicates the level of charm that has been suggested by others if there is significant charm content in the proton [31]. (The same two curves are shown in Fig. 2 as a pair of light, solid curves.)

5.4 The highest energy neutrinos

Neutrinos associated with the GZK cutoff and especially neutrinos from decay of topological defects have extremely high energy, though the fluxes are low. Detectors with effective volumes significantly larger than a kilometer cubed would be desirable, e.g. radio detection [32, 33, 34] or air shower detectors with gigantic acceptance [35, 36].

Acknowledgments. I am grateful for helpful conversations with Chuck Dermer, George Frichter, Paolo Lipari, Al Mann, Ray Protheroe, Ina Sarcevic, Todor Stanev and Eli Waxman. This work is supported in part by the U.S. Department of Energy under Grant No. DE-FG02-91ER40626.

References

- [1] A. Bottino et al., *Astroparticle Physics* 3 (1995) 65 and 5 (1996) 333.
- [2] T.K. Gaisser, Francis Halzen and Todor Stanev, *Physics Reports* 258 (1995) 173.
- [3] Reviews of Particle Properties, *Phys. Rev. D* 54 (1996) 122. (An error in the labelling of the ordinate has been corrected here.)
- [4] M. Amenomori et al., *Ap.J.* 461 (1996) 408.
- [5] Karl Mannheim, *Astroparticle Physics* 3 (1995) 295.
- [6] R. Protheroe, astro-ph/9607165.
- [7] Jörg P. Rachen and Peter L. Biermann, *Astron. Astrophys.* 272 (1993) 161.
- [8] Colin A. Norman, Donald B. Melrose & Abraham Achterberg, *Ap. J.* 454 (1995) 60.
- [9] Hyesung Kang, Jörg P. Rachen & Peter L. Biermann, *Mon. Not. R. Astron. Soc.* 286 (1997) 257.
- [10] A. Dar & N.J. Shaviv, *Phys. Rev. Letters* 75 (1995) 3052.
- [11] V.S. Berezinsky, P. Blasi, & V.S. Ptuskin, INFN/TH-96/04 and 96/05, *Ap.J.* (to be published).
- [12] Eli Waxman & John Bahcall, *Phys. Rev. Letters* 78 (1997) 2292.

charm production even at ultra-high energy. I thank Paolo Lipari for reminding me of this.

- [13] G. Sigl, S. Lee, D.N. Schramm & P. Coppi, *Phys. Letters* B392 (1997) 129.
- [14] S. Yoshida & M. Teshima, *Prog. Theoretical Phys.* 89 (1993) 833.
- [15] T.K. Gaisser, Francis Halzen & Todor Stanev, in preparation.
- [16] Paolo Lipari & Todor Stanev, *Phys. Rev.* D44 (1991) 3543.
- [17] Raj Gandhi et al., *Astropart. Physics* 5 (1996) 81.
- [18] W. Lohmann, R. Kopp & R. Voss, CERN Yellow Report No. EP/85-03.
- [19] Stecker et al. *Phys. Rev. Letters* 66 (1991) 2697; 69 (1992) 2738(E).
- [20] A.P. Szabo & R.J. Protheroe, in *High Energy Neutrino Astrophysics*, eds. V.J. Stenger et al., World Scientific (Singapore) (1992) 24.
- [21] A.P. Szabo and R.J. Protheroe, *Astropart. Physics* 2 (1994) 375. The predictions of this paper are higher than those of the previous reference because of a different assumption about the strength of the magnetic field which leads to a higher acceleration rate for protons.
- [22] W. Rhode et al., *Astroparticle Physics* 4 (1996) 217.
- [23] F. Krennrich et al. (Whipple Collaboration) *Ap. J.* 481 (1997) 758.
- [24] F. Aharonian et al. (HEGRA Collaboration), astro-ph/9706019, submitted to *Astron. & Astrophysics*.
- [25] S.D. Hunter et al., *Ap.J.* 481 (1997) 205.
- [26] Todor Stanev, private communication.
- [27] Paolo Lipari, *Astroparticle Physics* **1**, 195 (1993).
- [28] Vivek Agrawal et al, *Phys. Rev.* **D53**, 1314 (1996).
- [29] Gary C. Hill, *Astroparticle Physics* 6 (1997) 215.
- [30] M. Thunman, G. Ingelman and P. Gondolo, *Astropart. Physics* 5 (1996) 309.
- [31] L.V. Volkova et al. *Nuovo Cimento* C10 (1987) 465.
- [32] George M. Frichter, John P. Ralston & Douglas McKay, *Phys. Rev.* D53 (1996) 1684.
- [33] P.B. Price, *Astroparticle Physics* 5 (1996) 43.
- [34] J.V. Jelley, *Astroparticle Physics* 5 (1996) 255 and references therein.
- [35] S. Yoshida, H. Dai, C.H. Jui and P. Sommers, *Ap. J.* 479 (1997) 547.
- [36] J.J. Blanco-Pillado, R.A. Vásquez & E. Zas, *Phys. Rev. Letters* 78 (1997) 3614.

FIGURES

Fig. 1. The high energy cosmic-ray spectrum. The assumed extragalactic component is indicated by the solid line above 10^{18} eV.

Fig. 2. Differential rate of ν -induced, upward muons per logarithmic interval of neutrino energy (per $\text{km}^2\text{-yr}$). The fluxes are integrated over the full 2π steradians from below the horizon, including the effect of neutrino absorption in the Earth.

Heavy solid line: atmospheric neutrinos from π - and K-decay;

Thin solid lines ($< 10^7$ GeV): “mimumum” [30] and “maximum” [31] estimates of prompt neutrinos;

Upper dotted line: ν from AGN cores—maximum allowed by Frejus limit [22] in calculation of [20];

Lower dotted line: ν from AGN cores without confinement [19];

Thin solid line (peak at 10^6 GeV) AGN jets from Ref. [6];

Thin dashed line: maximum allowed from clusters of galaxies if this is source of diffuse (extragalactic) γ -ray background [11];

Heavy dashed line: Galactic plane in the direction of the galactic center (0.73 sr) [25];

Heavy dotted line (peak at 10^5 GeV): GRB model of Ref. [12];

Upper thin solid line ($> 10^7$ GeV): neutrinos from topological defects [13];

Lower thin solid line ($> 10^7$ GeV): example of neutrinos from interactions of cosmic rays with the microwave background radiation (maximum red shift = 2; bright-phase index = 2) [14].

Fig. 3. Neutrino interaction length vs. energy (from Ref. [17]).

Fig. 4. Convolution of the predicted GRB flux of $\nu_\mu + \bar{\nu}_\mu$ [12] with $P_\nu \times$ detector area (upper panel, arbitrary units) and the corresponding response curve (lower panel), which shows the relative contribution of neutrinos of different energies to the predicted signal of upward muons. The dashed curve in the lower panel shows the signal when absorption of high-energy neutrinos in the Earth is neglected, while the solid curve includes the effect of absorption.

Fig. 5. Muon range vs. energy (left solid curve). The right curve illustrates the relation between muon energy at production and at the detector (see text).

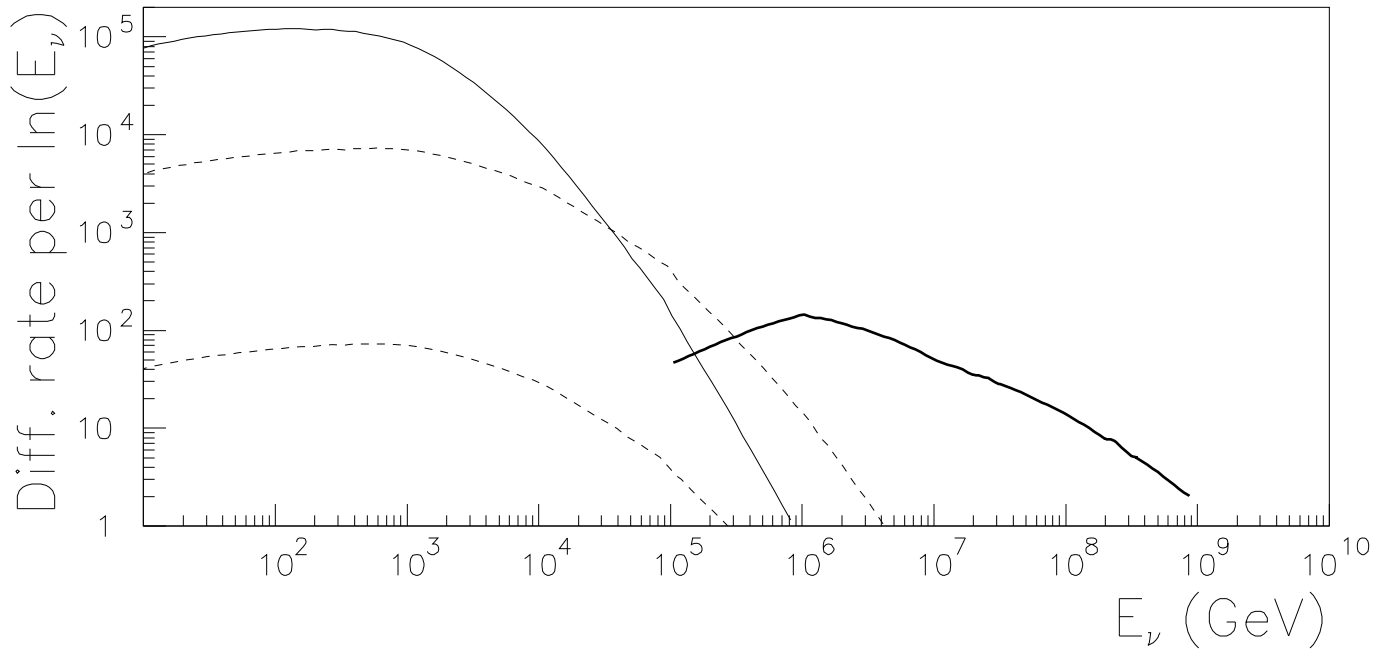
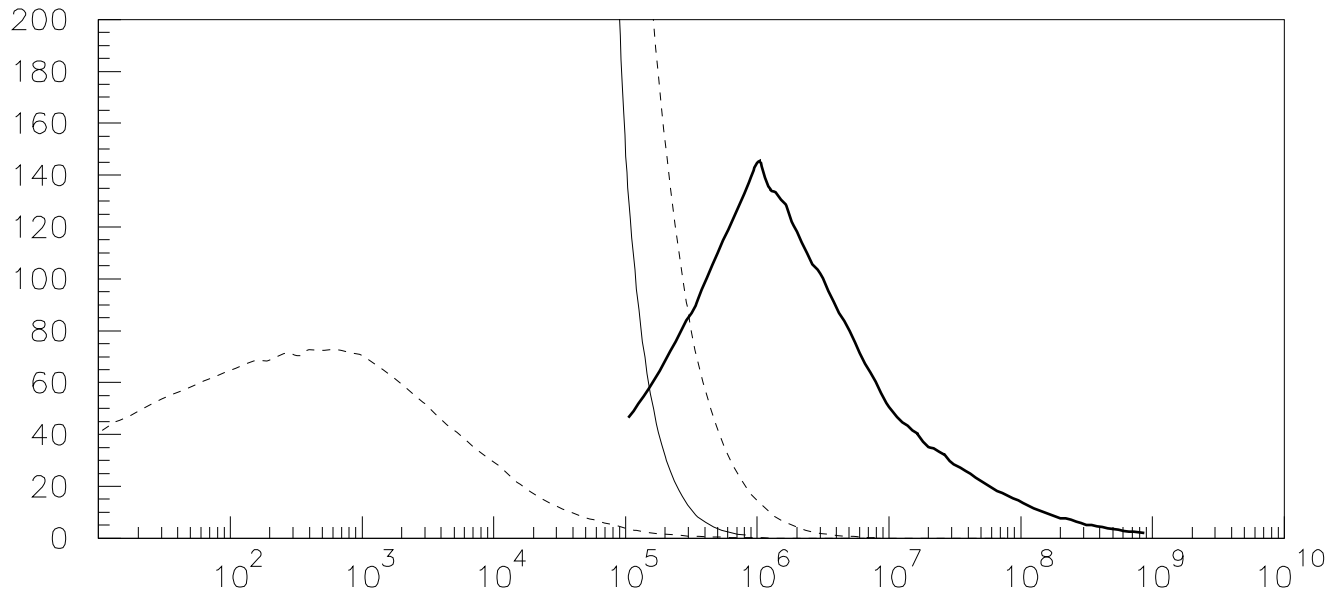
Fig. 6. Differential rate of neutrino-induced muons per logarithmic interval of parent neutrino energy for the AGN jet calculation of Ref. [6]. The thin solid line is the atmospheric background from decay of pions and kaons and the dashed lines are minimal [30] and maximal [31] estimates of prompt neutrinos. The same information is shown in both panels (upper with linear scale and lower with logarithmic).

Fig. 7. History of a single 10 TeV muon propagating through one kilometer of water. Scale can be read as GeV per burst (see text). Upper and lower panels show the history of the same muon on linear and logarithmic scales respectively.

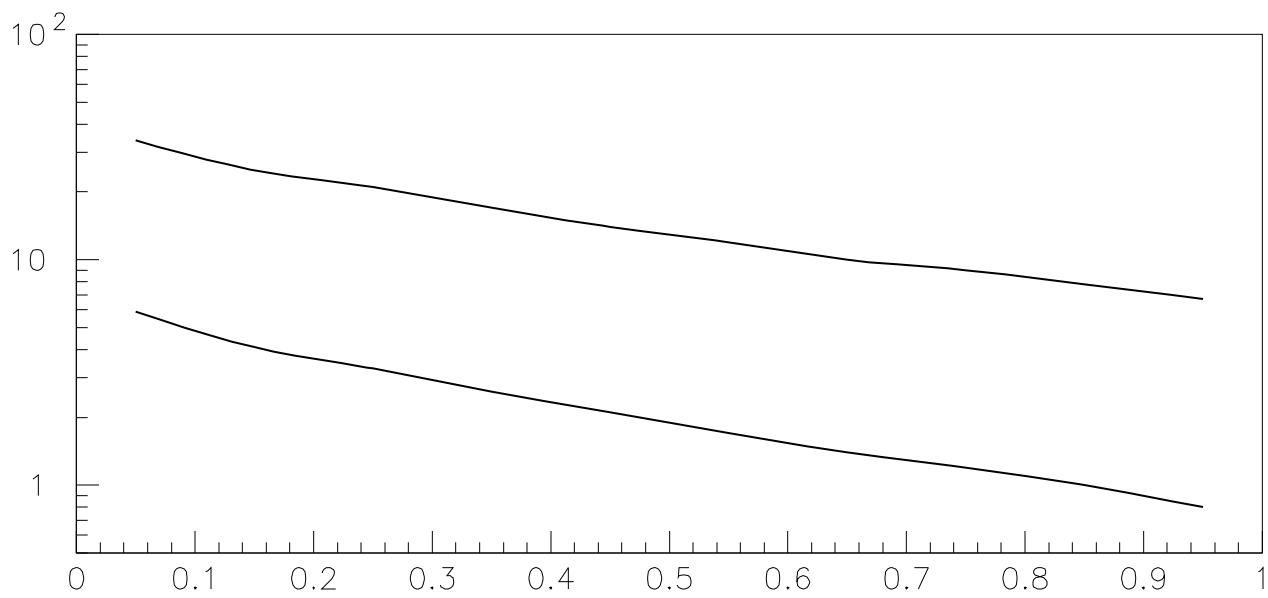
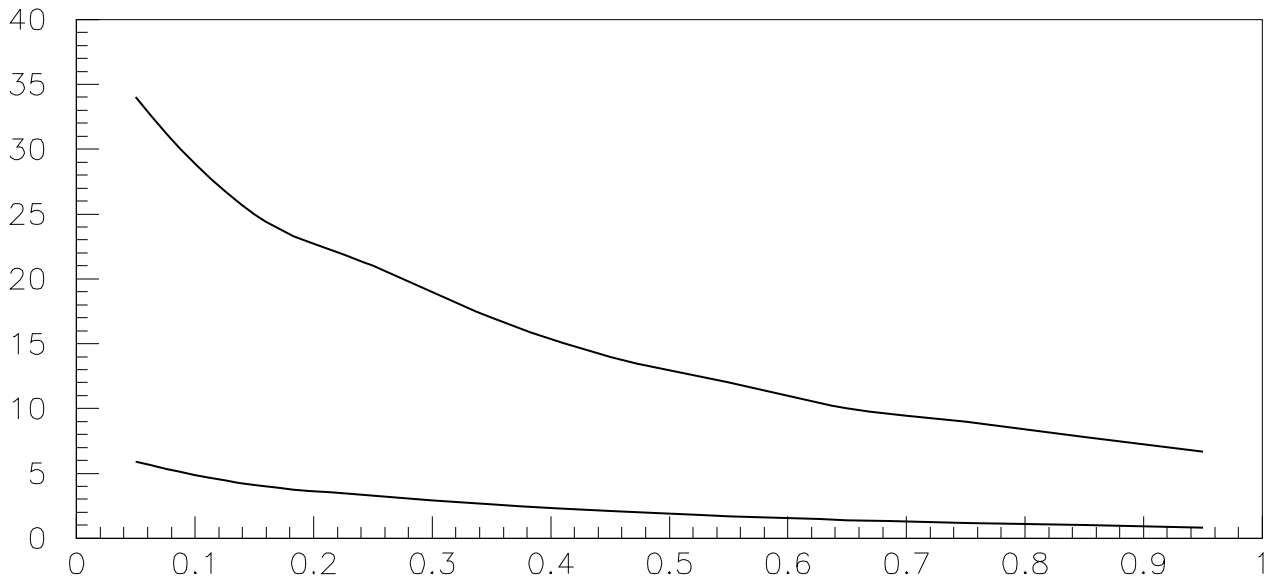
Fig. 8. Same as Fig. 6 for a 100 TeV muon.

Fig. 9. Angular dependence of upward, ν_μ -induced muons. The same information is shown on linear and logarithmic scales in the upper and lower panels. In each case the upper curve is for $E_\mu > 1$ TeV and the lower for $E_\mu > 3$ TeV. The scale is events per year per bin of $\Delta \cos \theta = 0.1$ in a projected area of 2×10^4 m².

6. Diffuse Blazar Signal

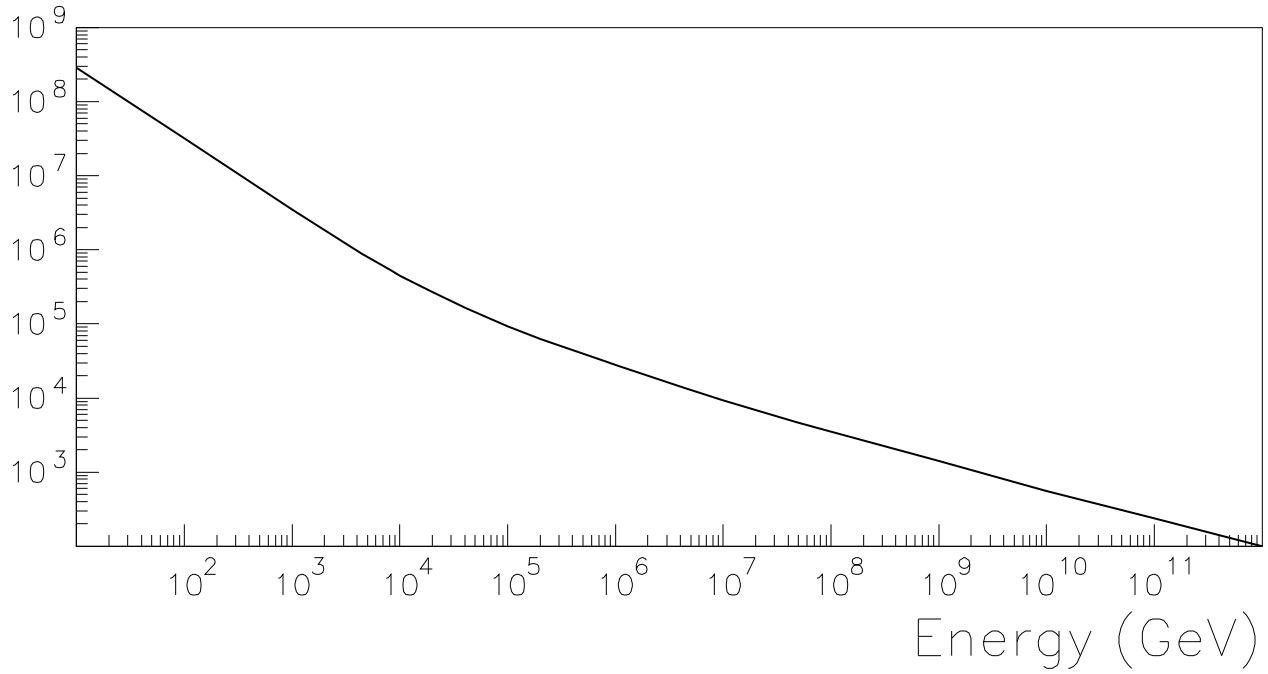


9. Upward muons from atmospheric neutrinos

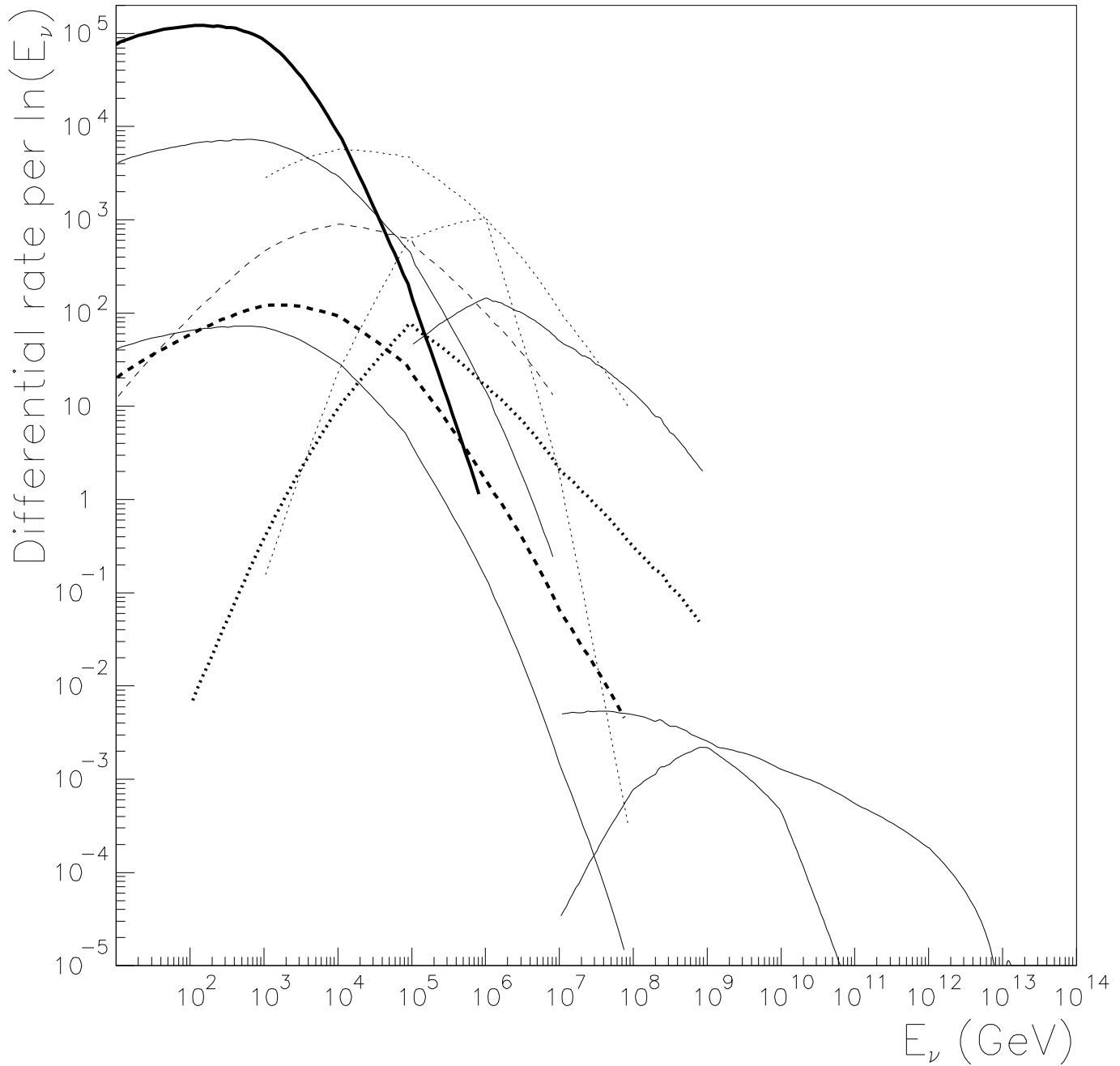


cosine nadir angle

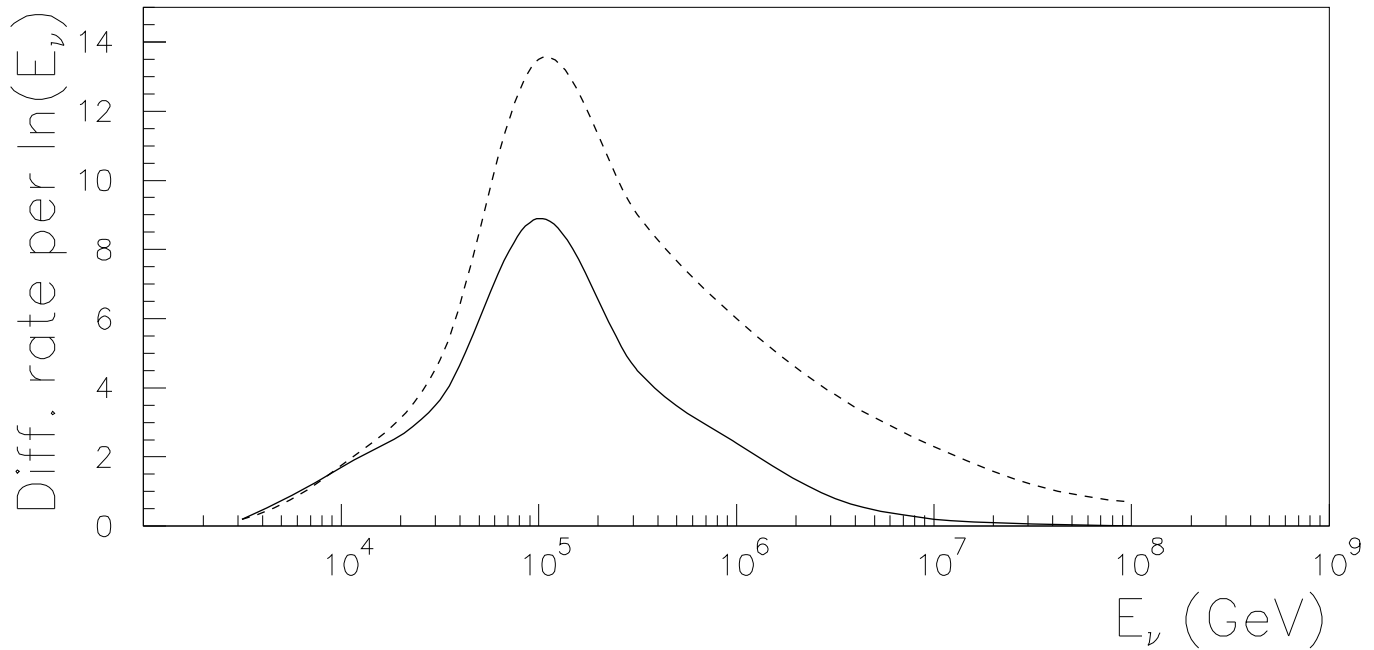
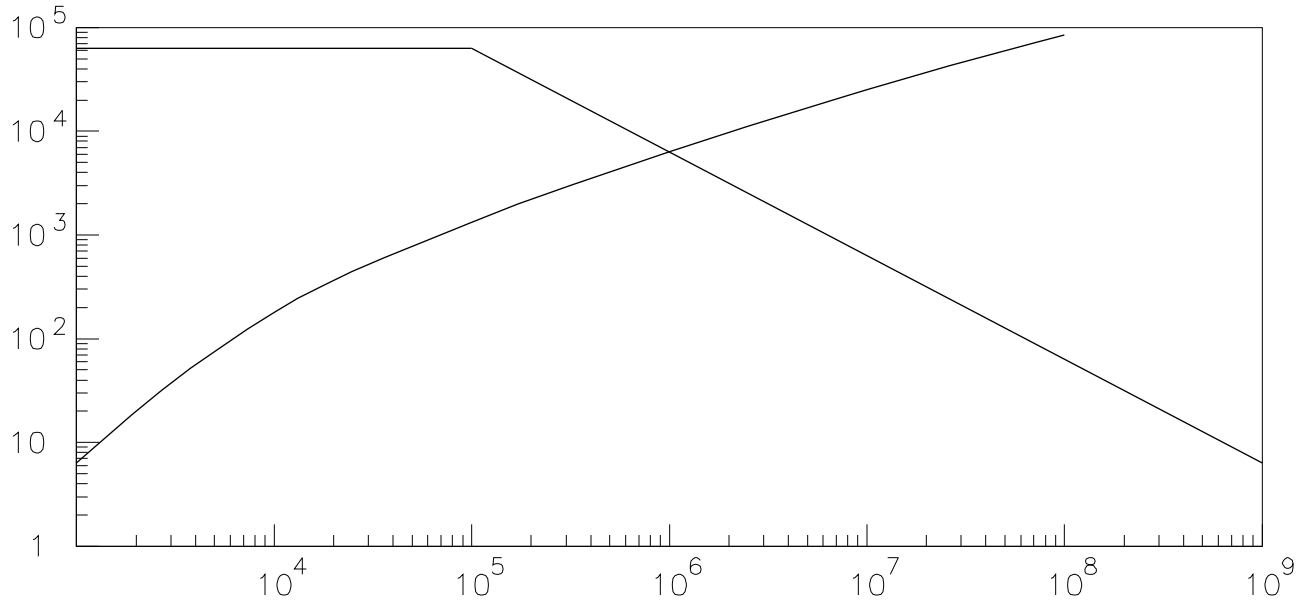
3. Neutrino interaction length (km.w.e.)



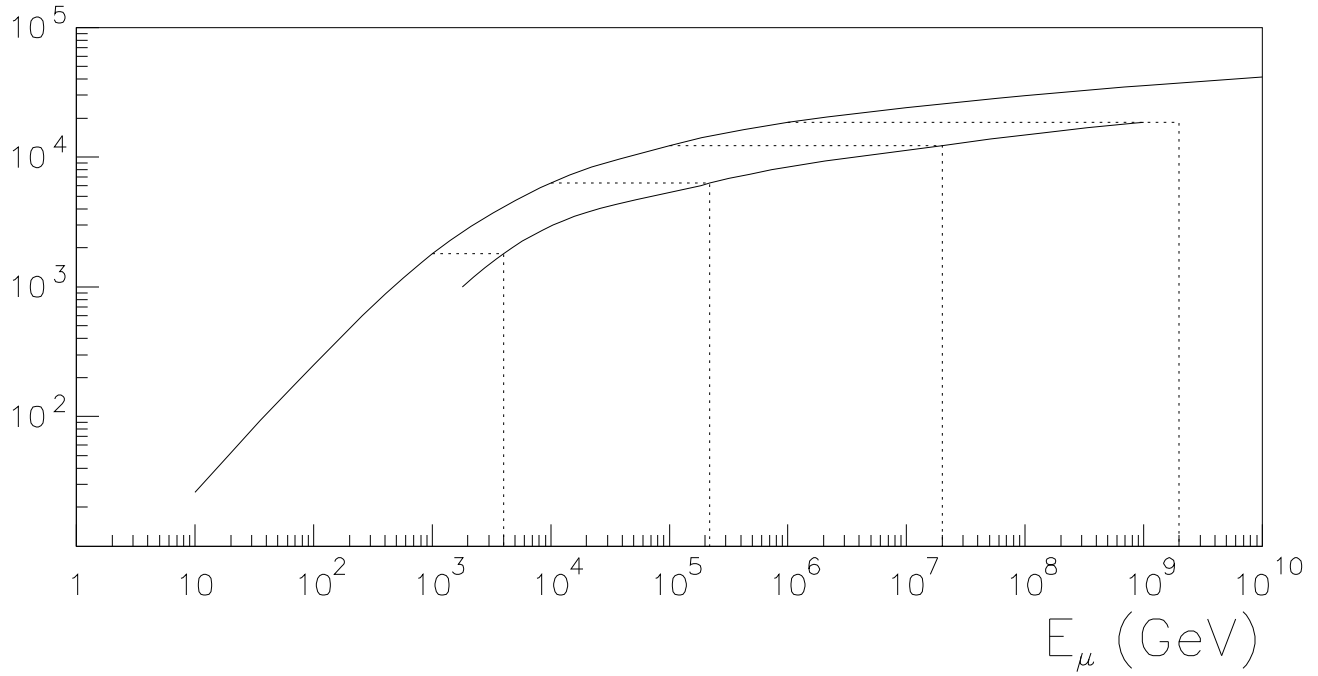
2. Rates of ν -induced $\mu^{+/-}$ per sq. km per year



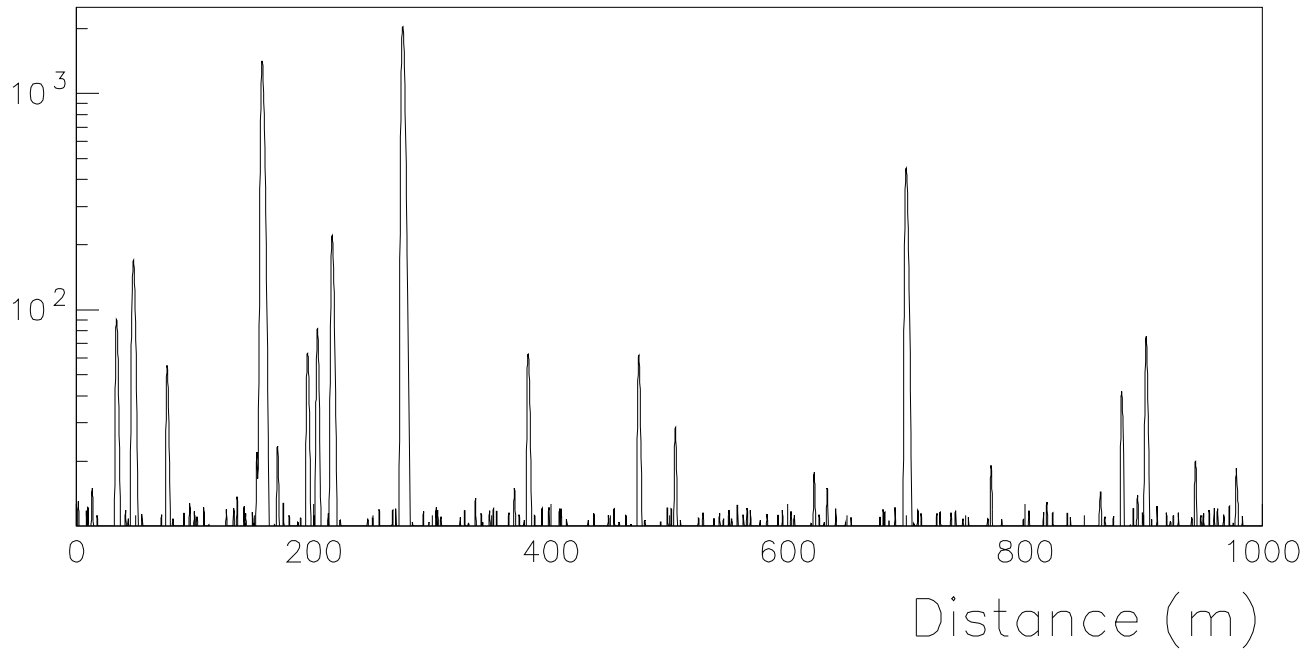
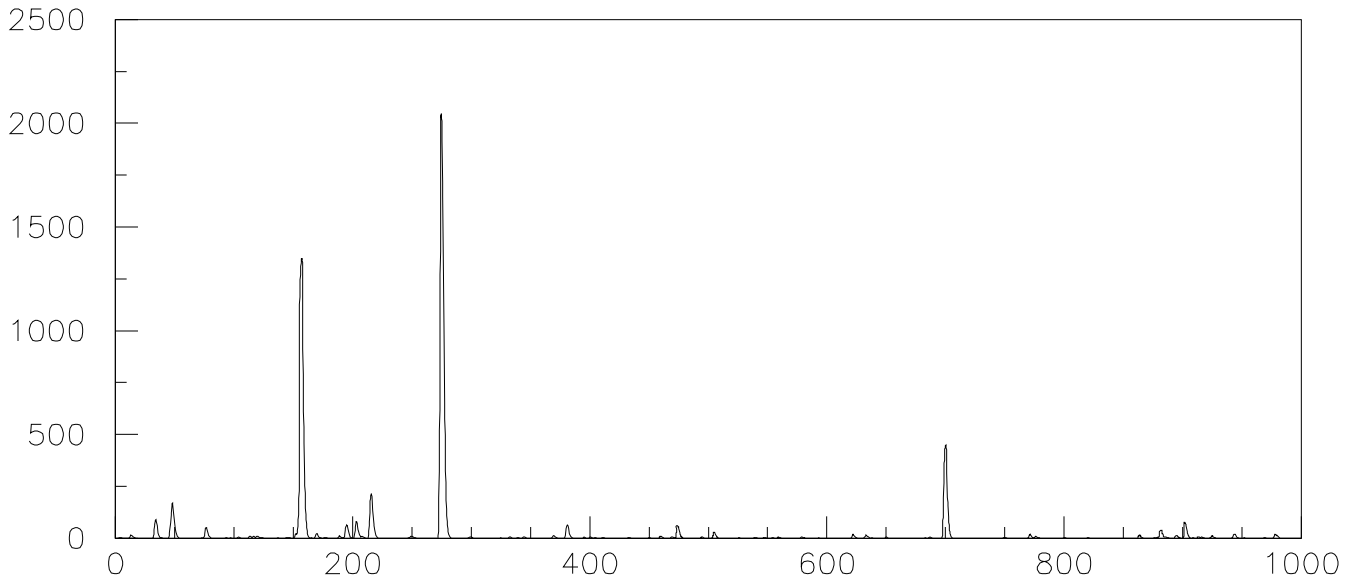
4. GRB flux times acceptance



5. Muon range (m)



7. SIZE for 10 TeV muon



8. SIZE for 100 TeV muon

